Hyper-PCN: Hypergraph-Based Point Cloud Completion via High-Order Correlation Modeling

Supplementary Material

7. More Results on KITTI

Following previous works, we report the quantitative results of MMD and FD on the KITTI dataset in Table 6. Although our method does not achieve the best numerical performance, it produces better visual results; additional visualizations are shown in Figure 8. It is worth noting that the KITTI dataset lacks ground truth, therefore the quantitative metrics are computed using reference point clouds sampled from the PCN dataset, and distribution differences between the two datasets may affect the accuracy of these metrics. Consequently, we place more emphasis on visual evaluation and consider the results on the ShapeNet-21 unseen subset to better reflect the model's generalization ability.

Table 6. Quantitative comparison on the KITTI dataset in terms of Fidelity Distance (FD) and Minimal Matching Distance (MMD)

Methods	PoinTr	SeedFormer	SVDFormer	Ours
FD (↓)	**0.0**	1.45	11.3	1.25
MMD (↓)	8.21	1.09	**0.97**	3.42

8. Additional Ablation Studies

Additional Ablation Studies on HyperRS To investigate the sensitivity of HyperRS to the filtering thresholds, we ablate the start and end thresholds $(\tau_{\text{start}}, \tau_{\text{end}})$. As reported in Table 7, setting $(\tau_{\text{start}}, \tau_{\text{end}}) = (0.2, 0.16)$ achieves the best trade-off among all configurations, with a CD of 6.20 and an F1 score of 0.858. A smaller threshold pair $(0.1, 0.06)$ is less effective at suppressing noisy responses, while larger thresholds such as $(0.3, 0.26)$ and $(0.4, 0.26)$ tend to over-filter fine structures, both leading to performance degradation. These results indicate that using a moderate level of thresholding in HyperRS is crucial for balancing noise suppression and the preservation of geometric details.

Table 7. Ablation studies on the HyperRS thresholds $(\tau_{\text{start}}, \tau_{\text{end}})$.

$(\tau_{\text{start}}, \tau_{\text{end}})$	CD (↓)	F1 (↑)
(0.1, 0.06)	6.22	0.855
(0.2, 0.16)	**6.20**	**0.858**
(0.3, 0.26)	6.24	0.853
(0.4, 0.26)	6.25	0.851

Additional Ablation Studies on A-HGNN We further ablate the number of neighbors used in the two A-HGNNs, denoted as $(\text{Topk}_1, \text{Topk}_2)$. As shown in the Table 8, setting $(\text{Topk}_1, \text{Topk}_2) = (24, 36)$ yields the best performance, achieving a CD of 6.20 and an F1 score of 0.858. A smaller neighborhood size $(12, 18)$ is insufficient to capture rich high-order relations, leading to slightly worse reconstruction quality. In contrast, larger settings such as $(36, 48)$ and $(48, 72)$ introduce redundant or noisy connections, which also cause mild performance degradation. These results suggest that choosing a moderate number of neighbors for the two anchor hypergraphs strikes a better balance between contextual aggregation and noise suppression.

Table 8. Ablation studies on the top-k neighbors of A-HGNNs.

$(Topk_1, Topk_2)$	CD (↓)	F1 (↑)
(12, 18)	6.23	0.853
(24, 36)	**6.20**	**0.858**
(36, 48)	6.22	0.854
(48, 72)	6.24	0.851

9. Discussion on the Advantage of Hypergraph

Conceptual Motivation Conventional graph convolution models relationships through pair-wise interactions. In point cloud completion, missing regions frequently break such pair-wise connectivity, limiting reliable information propagation. Hypergraph learning, in contrast, explicitly models group-wise, high-order correlations by connecting a set of vertices within a single hyperedge. Even if parts of a structure are missing, the remaining pieces can still form a hyperedge, allowing the network to infer the properties of the missing geometry from the group context.

Ablation Design and Empirical Validation We conduct a comparative study by replacing HyperRS and A-HGNN modules with standard, widely-used counterparts, while maintaining a comparable computational budget to ensure fairness:

- GCN-based: We replace hypergraph convolution with graph convolution in these modules to represent pair-wise correlations. To ensure a fair comparison, we employ the same graph construction strategy as our method.
- Set Abstraction-based: We replace the modules with PointNet or PointNeXt.

The results on PCN dataset are shown in Table 9. Despite using comparable or larger model capacity, both GCN- and SA-based variants underperform the proposed hypergraph-based design. We further increase the stacking depth of GCN layers within HyperRS and observe a bit improvement when L=12. Nevertheless, the GCN-based variant still exhibits a clear gap compared to the hypergraph-based design, suggesting that explicit group-wise modeling is more effective than deep stacks of pair-wise convolutions.

Table 9. Ablation of core modules by replacement.

(a) HyperRS.

Base	FLOPs(G)	Params(M)	CD(↓)
GCN (L=6)	6.47	12.61	6.28
GCN (L=12)	12.94	25.22	6.27
GCN (L=18)	19.41	37.83	6.33
PointNet	17.24	2.11	6.29
PointNeXt	146.42	17.85	6.35
Ours	**3.23**	**6.31**	**6.20**

(b) A-HGNN.

Base	FLOPs(G)	Params(M)	CD(↓)
GCN	25.82	2.10	6.26
PointNet	12.93	1.06	6.36
PointNeXt	13.84	1.12	6.39
Ours	**0.54**	**1.05**	**6.20**

10. Additional Visualizations

Additional Visualizations on PCN dataset We provide some additional visualization results on the PCN dataset (Figure 9 and Figure 10). The results show that HyperPCN can generate high-quality completed point clouds in various complex scenarios, accurately restoring details and structure.

Additional Visualizations of HyperRS In addition, we present more visualizations of the hyperedges in the HyperRS across different objects. Figure 11 illustrates HyperRS's hyperedge connections on different objects, further validating HyperRS's effectiveness in mining high-order correlation information from incomplete point clouds.

Additional Visualizations of A-HGNN To validate A-HGNN's effectiveness in capturing global high-order correlations, we visualized the hyperedges formed by anchor connections in the two A-HGNN modules in the encoder, as shown in Figure 12. Regions of the same color indicate the point sets connected by the same anchor. It can be observed that A-HGNN's hyperedges mainly connect the edge parts of neighboring missing regions, and the connected regions of the two A-HGNN modules are partly complementary; together they cover the edge information of missing regions across the whole shape. The edges of missing regions typically contain rich structural cues and semantic information that are crucial for inferring the shape and details of the missing parts. Through anchor-guided hypergraph construction, A-HGNN can effectively capture these global high-order correlations, thereby improving the quality and consistency of point cloud completion.

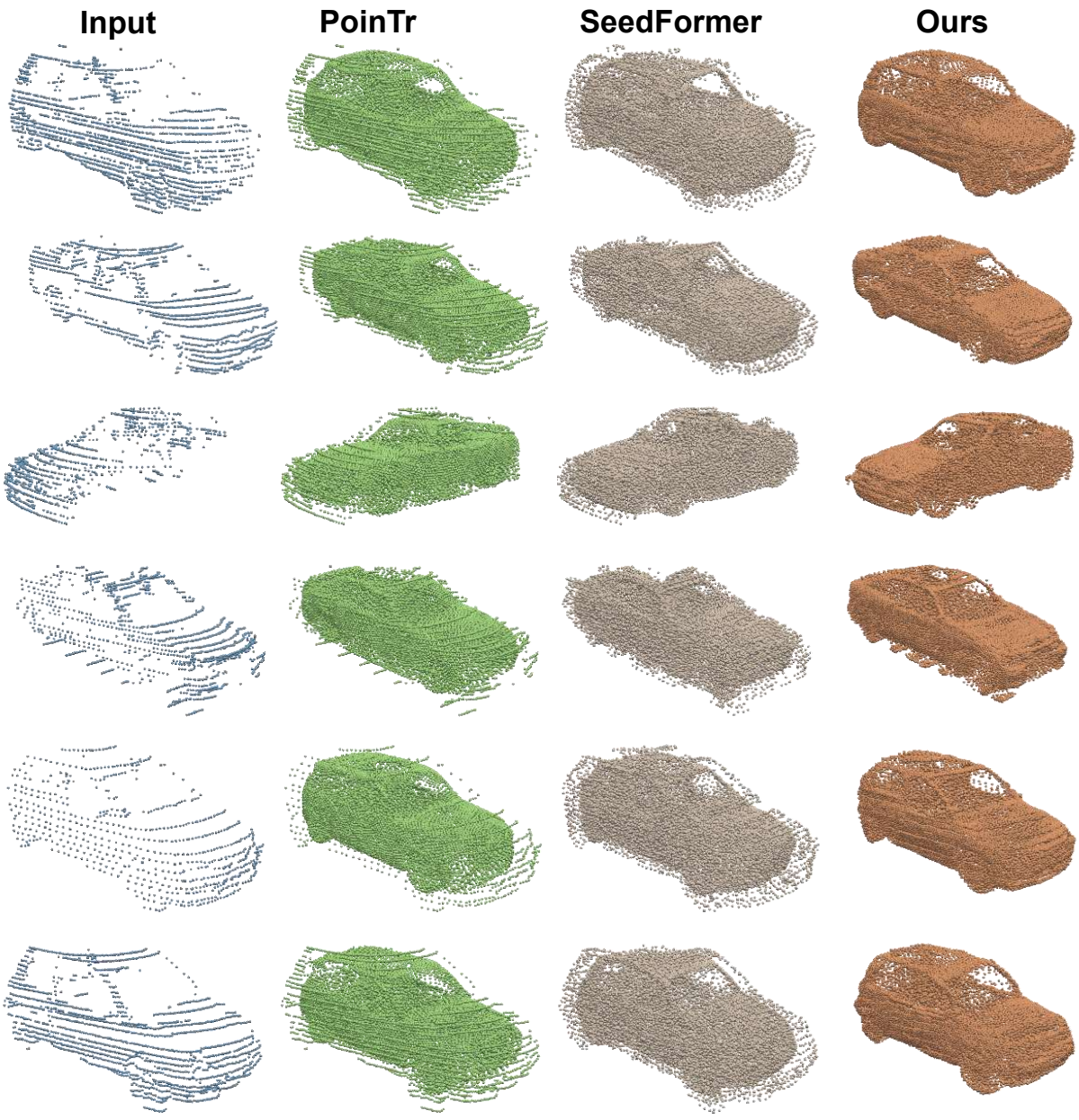

Figure 8. Additional visualizations on KITTI dataset.

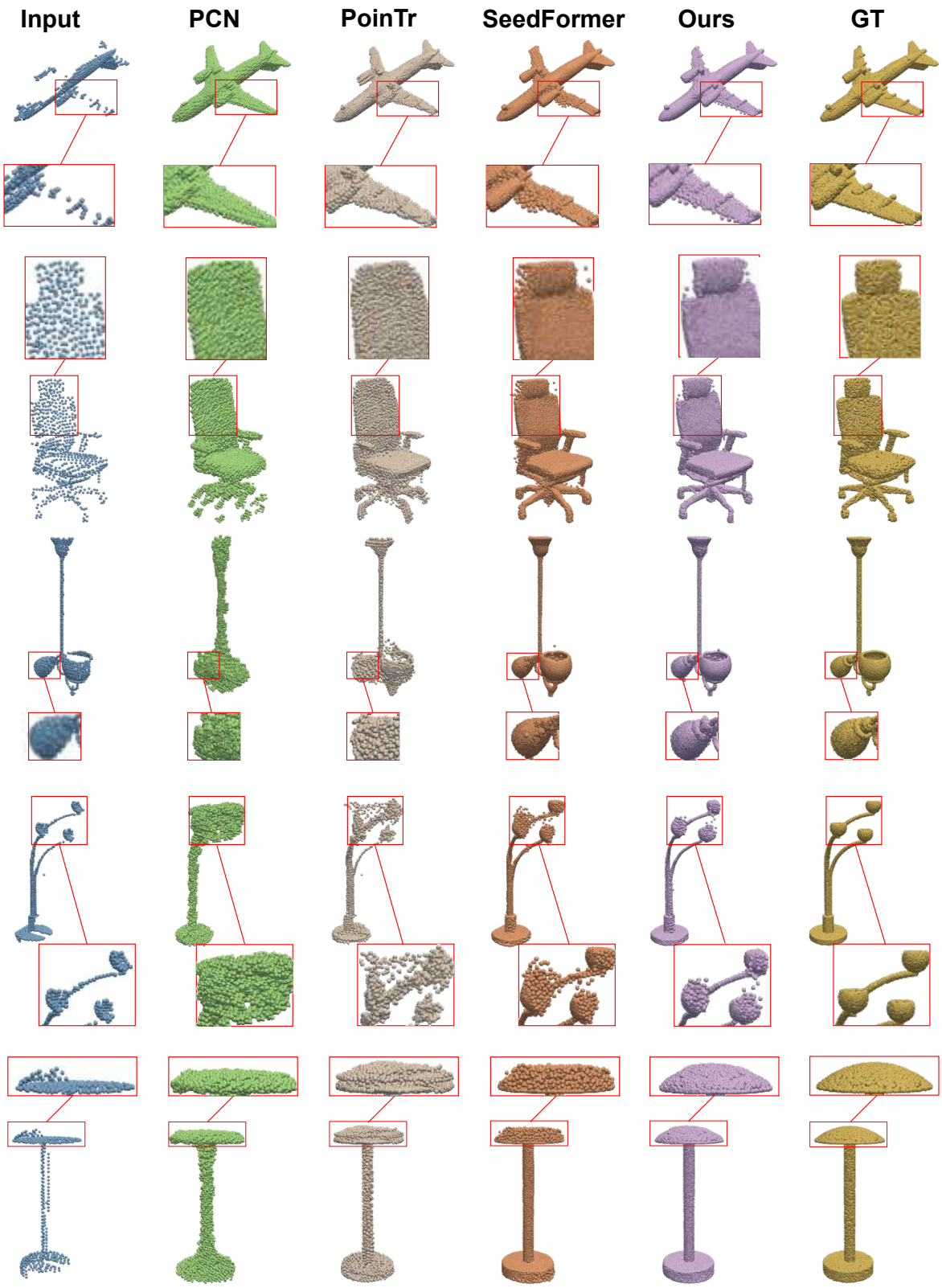

Figure 9. Additional visualizations on PCN dataset.

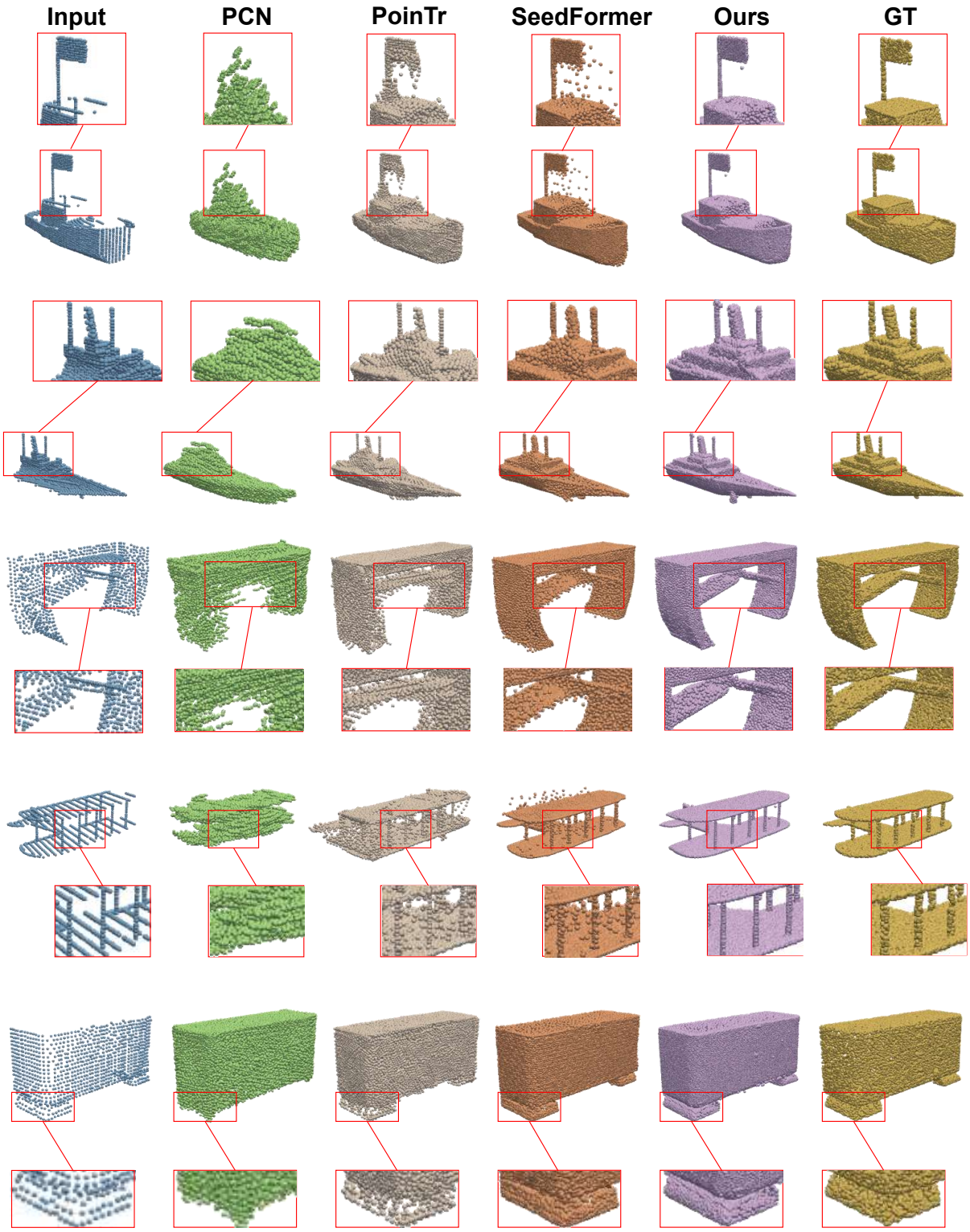

Figure 10. Additional visualizations on PCN dataset.

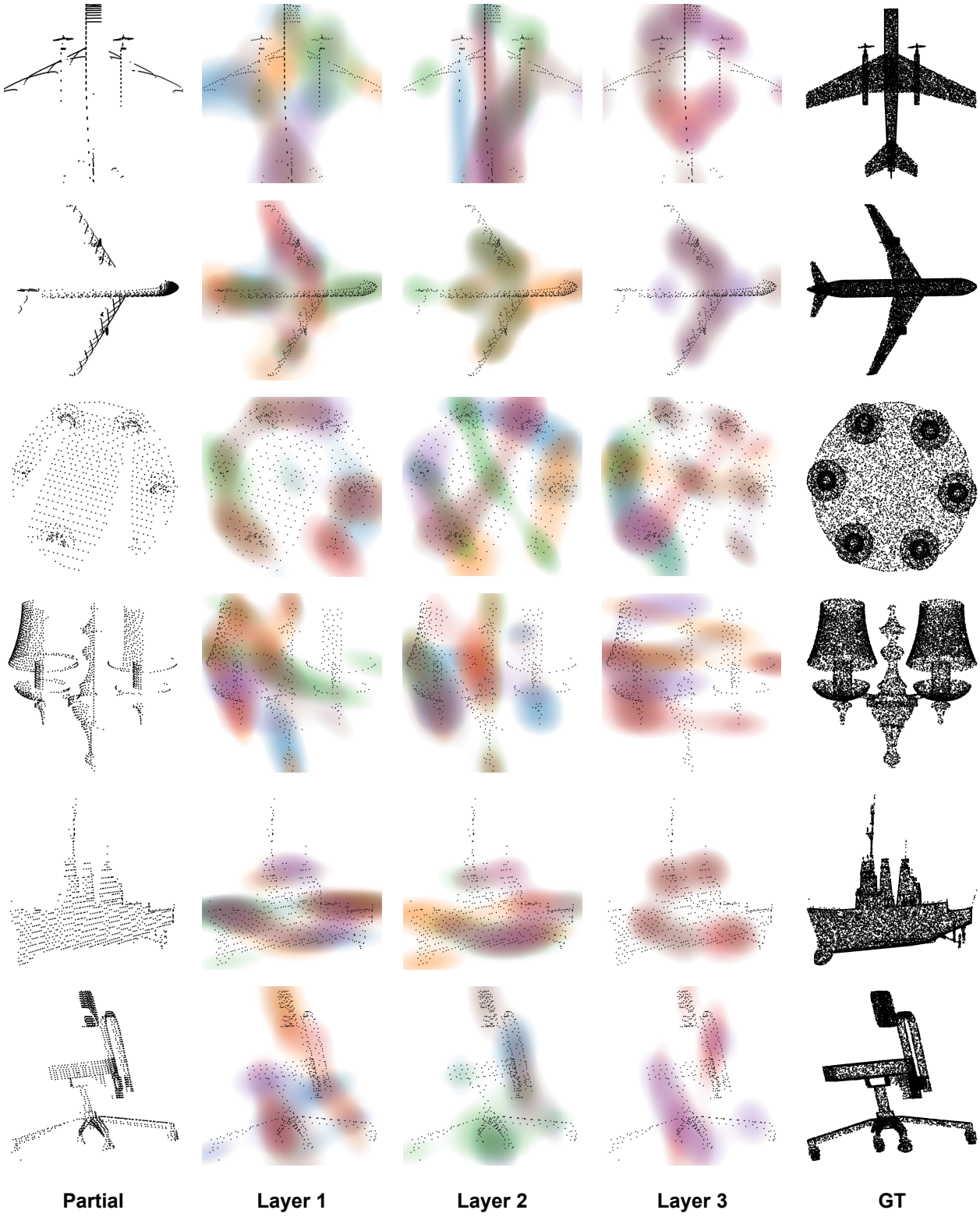

Figure 11. Additional visualizations of hyperedges in *Hyper Refinement Stack* layers.

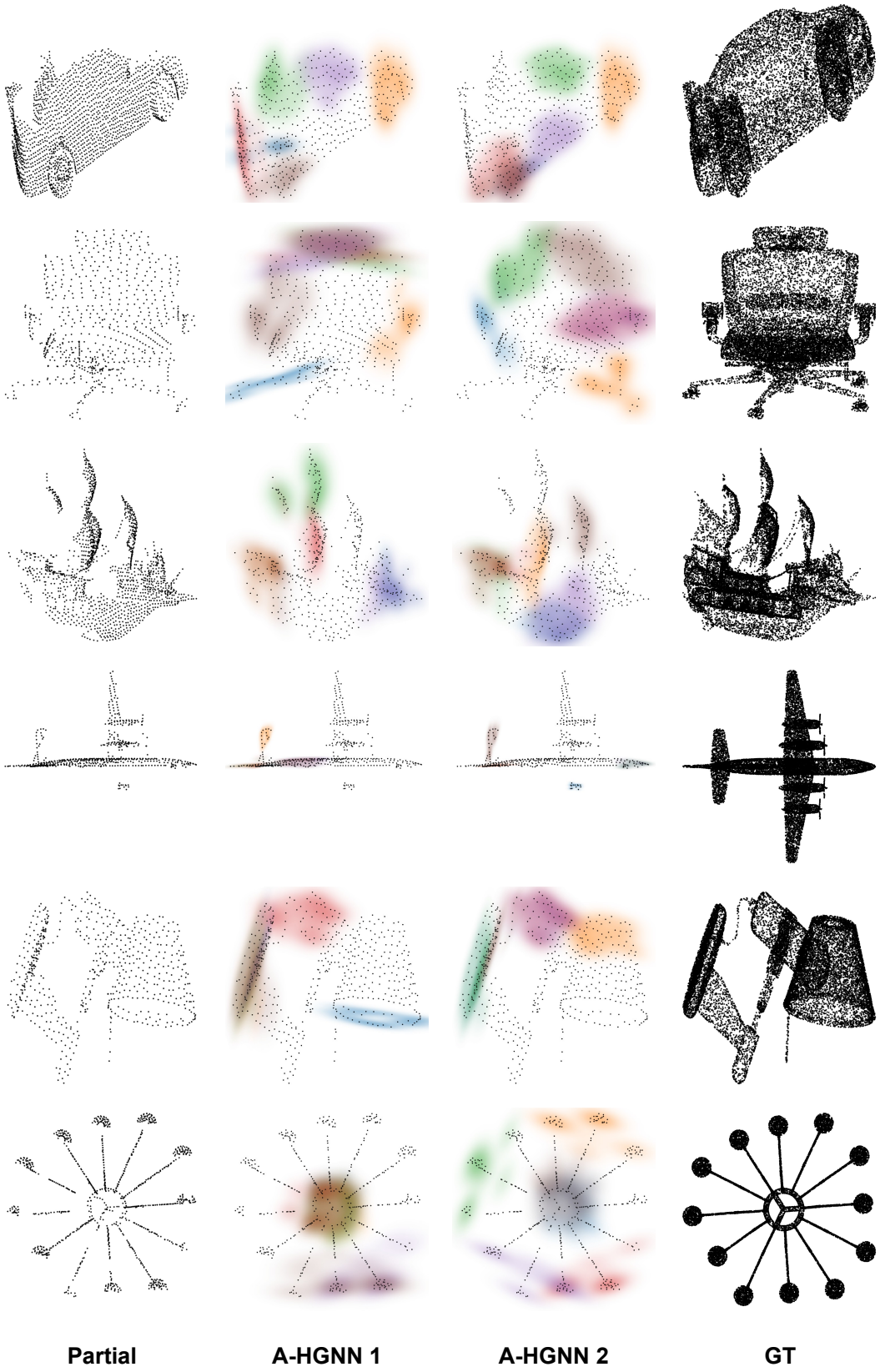

Figure 12. Additional visualizations of hyperedges in *A-HGNN*s.